Organic Electronics 14 (2013) 1744–1748

Contents lists available at SciVerse ScienceDirect

Organic Electronics

journal homepage: www.elsevier.com/locate/orgel

Letter

Key factors to improve the efficiency of roll-to-roll printed organic photovoltaics

Christos Koidis, Stergios Logothetidis *, Apostolos Ioakeimidis, Argiris Laskarakis, Christos Kapnopoulos

Aristotle University of Thessaloniki, Physics Department, Lab for Thin Films-Nanosystems and Nanometrology (LTFN), GR-54124 Thessaloniki, Greece

ARTICLE INFO

Article history:
Received 16 January 2013
Received in revised form 29 March 2013
Accepted 5 April 2013
Available online 19 April 2013

Keywords:
Roll-to-roll gravure
Flexible organic photovoltaics
Spectroscopic ellipsometry
Phase separation
Roll-to-roll drying
Printed P3HT:PCBM

ABSTRACT

In order to achieve the cost-efficient scalability of flexible organic photovoltaics (OPVs), the optimization of key factors related to the materials and roll-to-roll (R2R) processes is necessary. The limited drying during the R2R printing process induces a vertical phase separation leading to the formation of a P3HT-rich top region on the photoactive layer which acts as an electron barrier in normal geometry. We show that the increase of R2R drying time and/or post-annealing can enhance the OPV efficiency by the diffusion of PCBM towards the photoactive layer surface forming an electron transport network. It is estimated that the volume fraction of PCBM at the top region of the films triples from about 9% to 30%. In addition, the direct exposure of PEDOT:PSS to air after printing leads to morphological changes that negatively affect the efficiency. Therefore, the protection of PEDOT:PSS from air in combination to the increase of the R2R drying time enables the significant increase of the R2R printed OPVs efficiency to 1%.

1. Introduction

The rapid printing of precise features and uniform thin films by roll-to-roll (R2R) processes is of great importance in organic electronics [1]. Various printing technologies have been developed for R2R processes including slot-die and screen printing [2]. However, gravure can achieve both high precision and throughput in a R2R process [3].

In the case of flexible organic photovoltaics (OPVs), there are many parameters that affect their efficiency such as the morphology of the photoactive poly(3-hexylthiophene):(6,6)-phenyl C61 butyric acid methyl ester (P3HT:PCBM) layer [4] and the vulnerability of the constituent layers to air, contaminations and impurities [5]. Although there are some publications on the investigation and optimization of sheet-to-sheet gravure printed OPVs [6,7], there is a lack of reports on R2R gravure printed OPVs. In this letter, we report on the effect of key factors in R2R printing, that include sufficient R2R drying, annealing and the protection of poly(3,4-ethylenedioxythiophene):poly(styrenesulfonate) (PEDOT:PSS) layer from air, on the performance and functionality of R2R gravure printed OPV devices. A normal OPV geometry is more convenient when preparing devices for layers testing but in general it is undesirable for a large-scale production due to the vacuum processing steps. However, in order to focus on the properties of the photoactive layer and to investigate the effect of the R2R drying stage (in combination to post-annealing and PEDOT:PSS protection from air) on the P3HT:PCBM morphology, it was considered appropriate to adopt the simpler normal geometry where two layers of the OPV stack (PEDOT:PSS and P3HT:PCBM) are R2R printed.

2. Materials and methods

A Rotary Koater (RK Print Coat Instruments Ltd.) was used to print the photoactive P3HT:PCBM (P3HT: Rieke Metals, PCBM: Solenne BV) and PEDOT:PSS (ready-to-use

* Corresponding author. Tel.: +30 2310 998174.
E-mail address: logot@auth.gr (S. Logothetidis).

1566-1199/$ - see front matter © 2013 Elsevier B.V. All rights reserved.
http://dx.doi.org/10.1016/j.orgel.2013.04.015

Clevios™ FET from Heraeus) thin films on indium tin oxide (ITO)/polyethylene terephthalate (PET) substrates (OC50, 50 Ω/sq). PEDOT:PSS was printed at 3.7 m/min and dried for 19 s during the R2R process. One part of the PEDOT:PSS-printed roll was kept inside a glove box to be protected from the atmosphere, before the printing of the photoactive layer. In Table 1 the materials characteristics and the R2R process parameters are summarized. The photo current density–voltage (J–V) curves of the fabricated OPVs were measured using a Keithley 2420 source under AM 1.5G and 100 mW/cm^2 of irradiation using a Newport solar simulator (91191).

The induced phase separation in the P3HT:PCBM films during R2R printing was investigated by the calculation of the % volume fraction of the blend components at the top (X_t, X = P3HT, PCBM) and bottom (X_b, X = P3HT, PCBM) region of the photoactive layers through the analysis of the pseudo-dielectric functions $\langle\varepsilon(\omega)\rangle$ measured by Spectroscopic Ellipsometry (SE) (1.5–6.5 eV) (Horiba Scientific), as it is described elsewhere [8,9]. The morphology of the printed films was investigated by Atomic Force Microscopy (AFM) (NTEGRA by NT-MDT), while the structural properties were examined by X-ray Diffraction (XRD) (Siemens D-5000). Finally, the surface energy of the PEDOT:PSS film was calculated by Contact Angle (CA) (CAM200 from KSV Instruments Ltd.) [8], and the conductivity by the standard Van der Pauw DC method.

3. Results and discussion

During R2R printing, using a typical speed of 3.7 m/min, the wet P3HT:PCBM films are dried for t_{R2R} = 19 s (dryer active length of 120 cm). Due to this limited drying time an amount of 1,2-dichlorobenzene (o-DCB) is not evaporated from the films during the drying, but it evaporates slowly after the end of the drying stage (slow-drying process) [8]. This results to the spatial rearrangement of P3HT chains and the fullerene molecules. More specifically, P3HT chains self-assemble and form crystallites with a-axis orientation [10], whereas at the same time, the PCBM molecules diffuse towards the bottom interface with PEDOT:PSS, and towards the surface forming PCBM nanocrystals [8,11]. This vertical phase separation is attributed to the differences in the surface energy of pristine P3HT (24 mN/m) and PCBM (38 mN/m) and the induced dipole–dipole interactions between PCBM and the PEDOT:PSS [9].

Post-annealing is expected to speed-up the crystallization of P3HT and lead to a better interfacial contact between the photoactive layer and the cathode [12]. In Table 2 the size of the P3HT crystallites (D_{P3HT}) is shown, calculated by the Scherrer formula [13]. The A1 sample, that is not annealed (t_{an} = 0) but only slow-dried during the R2R process, exhibits D_{P3HT} = 18.8 nm, whereas in A2 (t_{an} = 3 min) crystallites of D_{P3HT} = 20.1 nm are formed with enhanced stacking order. However, further annealing does not affect D_{P3HT} which gets saturated [14]. In addition, the gradual increase of t_{an} to 17 min (A1–A4) leads to the increase of the PCBM$_t$ from 8.6% (A1) to 29.5% (A4). This is combined with a gradual decrease of the PCBM$_b$ from 78.8% (A1) to 69.4% (A4), which indicates that PCBM is diffusing out even from the bottom region of the films. The increase of t_{R2R} to 60 s leads to the increase of the D_{P3HT} to 21.6 nm and the enhancement of crystallinity (B3).

As it is shown in the AFM nanotopography of the A1 sample in Fig. 1a, large material domains of more than 200 nm in width are observed, instead of the bi-continuous networks that can lead to the efficient charge generation and transport [15]. These domains are mostly attributed to the P3HT aggregation and result from the lateral phase separation (combined with the vertical one) during the slow-drying process [8]. The P3HT-rich content on the top region of the A1 film (P3HT$_t$ = 91.4%) acts as an electron injection barrier; PCBM exists mostly in the form of nanocrystals of about 50–100 nm in width, as they are clearly shown in the phase image of Fig. 1b. In that sense, the A1 OPV is not functional.

The annealing process leads gradually to a nanometer-scale morphology (contributed by the increase of the PCBM$_t$) (Fig. 1c), where P3HT crystallites, PCBM molecules and nanocrystals and the P3HT amorphous phase coexist [16]. The root mean square (rms) and peak-to-valley roughness of A4 increase to 1.2 and 13.5 nm, respectively, compared to the A1 which exhibits corresponding values of 0.6 and 5.1 nm. This increase is due to the change in morphology and the increase of the P3HT and PCBM crystal size. In particular, the size of the PCBM nanocrystals increases to about 50–150 nm in width and to about 4–6 nm in height, as it is shown in the cross section graph of Fig. 1e.

According to the J–V curves of Fig. 1f and the extracted electrical data collected in Table 2, the increase of t_{an} to 7 min (A3) leads to improved short circuit current density (J_{sc} = 2 mA/cm^2) and fill factor (FF = 25.40%) values, and power conversion efficiency (PCE) of 0.26%, which imply the improvement in charge carrier mobility assisted by the formation of a network for electron transport due to the continuing aggregation of PCBM on the top region of the films. Also, the increase of the open circuit voltage (V_{oc}) to 0.508 V indicates the improvement in the contact between the photoactive layer and the cathode [12]. For t_{an} = 17 min (A4), despite the further interface improvement indicated by the increase of V_{oc} to 0.528 V, the decrease of FF to 22.95% and J_{sc} to 1.89 mA/cm^2 is observed. In addition, the series resistance (R_s) of A4 is calculated to increase to 353 Ω cm^2 in relation to 239 Ω cm^2 of A3. These findings imply that from a point and on the segregation of PCBM on the top region of the film induced by the annealing process, despite being beneficial for the quality of the interface with the cathode, it is not beneficial for

Table 1
Summary of the materials and R2R process parameters.

P3HT:PCBM ratio/concentration	1:0.8/100 mg/ml
Solvent	1,2-Dichlorobenzene
Speed/nip pressure	3.7 m/min/45 psi
Screen/cells volume	80 lines/cm/12.7 ml/m^2
R2R drying/annealing temperature	140 °C/110 °C
P3HT:PCBM/PEDOT:PSS thickness	About 190 nm/50 nm
Cathode thickness Ca/Al	About 10 nm/100 nm
Device active area	0.5 cm^2

Table 2
The treatment conditions and the structural and electrical characteristics of the R2R printed OPVs A1–A4 and B1–B3.

Sample	PEDOT:PSS protection (yes/no)	t_{R2R} (s)	t_{an} (min)	$PCBM_t$ (%)	$PCBM_b$ (%)	D_{P3HT} (nm)	J_{sc} (mA/cm^2)	V_{oc} (V)	FF (%)	PCE (%)
A1	N	19	0	8.6 ± 2.0	78.8 ± 4.6	18.8	–	–	–	–
A2	N	19	3	16.6 ± 1.6	78.4 ± 4.3	20.1	0.67	0.487	21.90	0.07
A3	N	19	7	28.0 ± 1.1	74.1 ± 3.4	20.3	2.00	0.508	25.40	0.26
A4	N	19	17	29.5 ± 1.2	69.4 ± 3.7	20.8	1.89	0.528	22.95	0.23
B1	Y	19	7	24.5 ± 1.9	76.1 ± 2.6	21.2	3.10	0.550	25.32	0.43
B2	Y	60	7	27.5 ± 1.6	68.1 ± 2.3	21.4	5.28	0.535	31.06	0.88
B3	Y	60	12	26.6 ± 1.6	69.3 ± 2.3	21.6	5.68	0.553	31.94	1.00

the morphology and the efficient charge transport within the active layer.

However, despite the observed improvement in morphology by the annealing process, the efficiency remains limited. This means that post-annealing can only partially reverse the negative effect of the slow-drying process during R2R printing. Furthermore, the direct exposure of PEDOT:PSS to air right after the printing has a critical effect on the device performance. The surface energy of the PEDOT:PSS under air exposure is calculated to decrease within about half an hour after printing from about 58 to 53 mN/m (the surface energy in 24 h was calculated also at about 53 mN/m), which indicates that morphological changes take place in the film; PEDOT becomes less shielded by PSS and thus more susceptible towards the oxygen induced degradation. This reorganization of the molecules at the surface leads to the decrease of the work function of PEDOT:PSS by affecting either the carrier density in PEDOT:PSS near the surface or the formation of a dipole layer [5]. In Fig. 2 the AFM phase images of the PEDOT:PSS film right after printing (a) and after 24 h (b) are shown. The bright (positive degree in phase) and dark (negative degree in phase) regions in the AFM phase image of Fig. 2a correspond to the PEDOT-rich cores and the PSS-rich cells, respectively, and imply a phase-separated morphology with increased conductivity [17] (about 175 S/cm). On the contrary, the reorganization of the molecules under air exposure leads to a less distinct phase separation (Fig. 2b) and diminished conductivity (about 150 S/cm). In addition, the rms (peak-to-valley) roughness of the more conductive PEDOT:PSS film right after printing is calculated at 3.5 nm (24.5 nm), whereas the corresponding value after 24 h is 2.9 nm (22.0 nm). This small decrease of the roughness also indicates the morphological changes in the film due to air exposure.

In view of the above, the higher work function of the protected (in inert atmosphere) PEDOT:PSS (B1), in relation to the unprotected one (A3), leads to a higher V_{oc} (0.550 V for B1 instead of 0.508 V for A3) in combination to a higher J_{sc} (3.10 mA/cm^2 for B1 instead of 2.00 mA/cm^2 for A3) which gives an OPV PCE of 0.43%, as it is shown in Table 2. It is remarkable to mention also that the $PCBM_b$

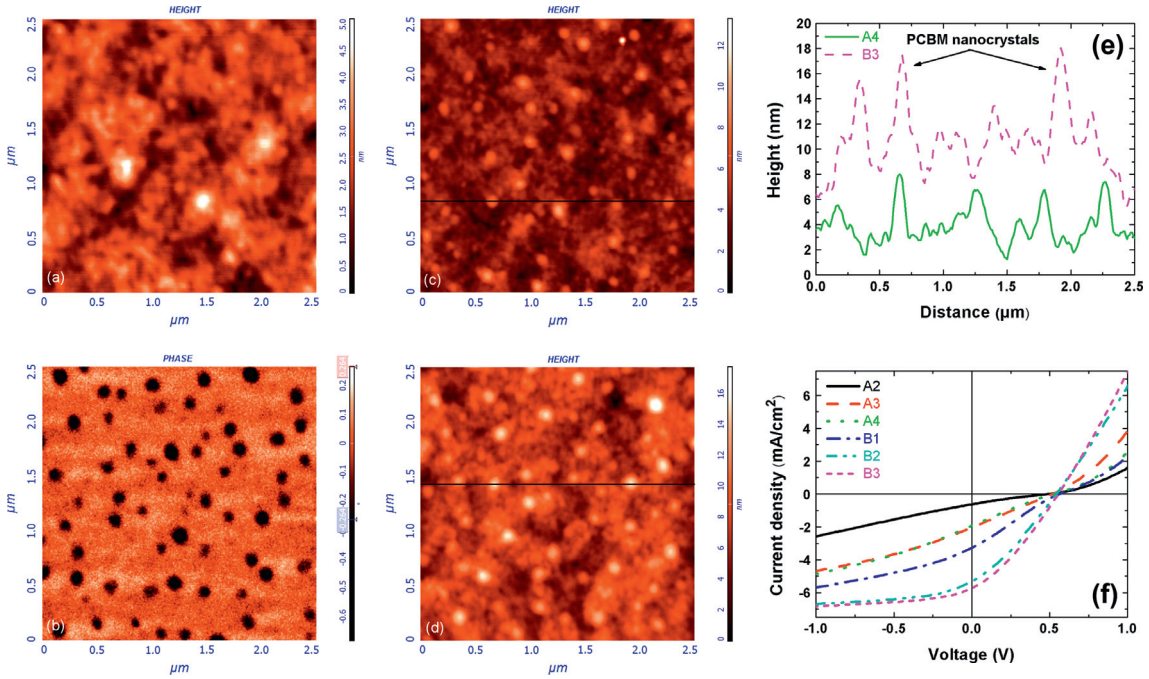

Fig. 1. The AFM nanotopography (a) and phase image (b) of the A1 P3HT:PCBM film. The AFM nanotopographies of the A4 (c) and B3 (d) P3HT:PCBM films. The cross section analysis graphs of the A4 and B3 P3HT:PCBM films (e). The cross sections are indicated by the black lines in 1c and 1d for A4 and B3, respectively. AFM scan size of 2.5 μm × 2.5 μm. The *J*–*V* characteristics of the R2R gravure printed OPVs (f).

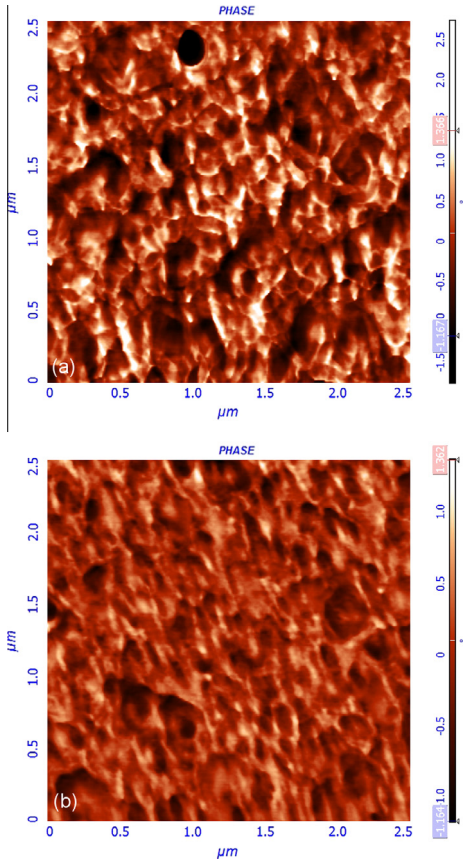

Fig. 2. The AFM phase images of the R2R printed PEDOT:PSS right after printing (a) and after 24 h (b). AFM scan size of 2.5 μm × 2.5 μm.

of the B1 is calculated slightly larger in relation to that of the A3 which is attributed to the higher surface energy of the (protected) PEDOT:PSS layer [9].

Both annealing and the protection of the PEDOT:PSS layer from air enable the enhancement of the PCE; nevertheless, in order to limit the vertical phase separation in the P3HT:PCBM layer during the R2R process, the increase of the t_{R2R} is necessary for the evaporation of the o-DCB and the restriction of the slow-drying process. Comparing B2 to B1 (Fig. 1f and Table 2), by applying t_{R2R} = 60 s instead of 19 s, the PCE is doubled from 0.43% to 0.88% due to the improvement of the morphology and the remarkable increase of the FF and J_{sc} from 25.32% to 31.06% and from 3.10 to 5.28 mA/cm^2, respectively. B2 is characterized by much better transport properties and extraction barriers, while in addition the segregation of PCBM in the bottom region of the film is significantly reduced (PCBM$_b$ = 68.1% for B2 instead of 76.1% for B1).

For t_{an} = 12 min (B3), the increase of the V_{oc} and the improvement in the contact between the photoactive layer and the cathode interface enables a PCE of 1%. As it is shown in Fig. 1d and e PCBM nanocrystals of about 100–150 nm in width and about 6–8 nm in height are formed. This, in combination with the increased D_{P3HT} drives to a rms (peak-to-valley) surface roughness of 2.0 nm (17.7 nm).

The vertical phase separation during R2R processing is more suitable for the inverted device geometry than normal one, since the P3HT-rich top region in the photoactive layer acts as a hole-transport layer and the PCBM-rich bottom region as an electron transport layer [18,19]. However, the extended phase separation may negatively affect the morphology and the formation of the efficient pathways for charge transport, which implies the necessity for the morphology control during the drying stage.

4. Conclusions

In this work, we reported on the effect of three critical parameters (t_{R2R}, t_{an}, PEDOT:PSS exposure to air) for the R2R printing of efficient OPVs towards large-scale fabrication.

The sufficient drying of the photoactive layer during the R2R processing is the most critical factor for the PCE improvement of the OPVs since it induces the enrichment of the photoactive layer top region with PCBM and leads to the formation of a bi-continuous network in the film. Contrarily, the limited R2R drying and the consequent slow-drying process in the photoactive layer leads to an undesirable morphology and to the vertical phase separation of the blend components. Annealing can also contribute to the efficiency enhancement (up to a point) mainly by the improvement of the photoactive layer/cathode interface in normal geometry OPVs. Our findings underline the importance of the optimization of the R2R drying stage and the control of the vertical distribution and morphology for the production of OPVs.

Except from the efficient control of the vertical segregation, especially during the R2R drying process, the protection of PEDOT:PSS from air during the printing process is another very important parameter that can substantially increase the efficiency. This implies that the use of an inert-atmosphere R2R equipment can contribute to the production of OPVs with enhanced efficiency.

Acknowledgements

This work has been partially supported by the National Strategic Reference Framework (NSRF) 2007-2013 under the Projects YFATRONIC (09SYN-82-747) and NanOrganic (09SYN-42-722), and the EC Project REGPOT-286022 ROle-Mak. The authors would like to thank C. Pitsalidis, M. Chatzidis and N.A. Hastas for the cathode evaporations, AFM measurements and conductivity measurements, respectively, and D. Georgiou and P.G. Karagiannidis for the fruitful discussions.

References

[1] F.C. Krebs, Fabrication and processing of polymer solar cells: a review of printing and coating techniques, Sol. Energy Mater. Sol. C. 93 (2009) 394–412.
[2] M. Manceau, D. Angmo, M. Jørgensen, F.C. Krebs, ITO-free flexible polymer solar cells: from small model devices to roll-to-roll processed large modules, Org. Electron. 12 (2011) 566–574.
[3] C.H. Kim, J. Jo, S.-H. Lee, Design of roll-to-roll printing equipment with multiple printing methods for multi-layer printing, Rev. Sci. Instrum. 83 (2012). 065001-1–065001-8.

[4] J.Y. Kim, S.H. Kim, H.-H. Lee, K. Lee, W. Ma, X. Gong, A.J. Heeger, New architecture for high-efficiency polymer photovoltaic cells using solution-based titanium oxide as an optical spacer, Adv. Mater. 18 (2006) 572–576.
[5] K. Norrman, M.V. Madsen, S.A. Gevorgyan, F.C. Krebs, Degradation patterns in water and oxygen of an Inverted polymer solar cell, J. Am. Chem. Soc. 132 (2010) 16883–16892.
[6] P. Kopola, T. Aernouts, S. Guillerez, H. Jin, M. Tuomikoski, A. Maaninen, J. Hast, High efficient plastic solar cells fabricated with a high-throughput gravure printing method, Sol. Energy Mater. Sol. C. 94 (2010) 1673–1680.
[7] M.M. Voigt, R.C.I. Mackenzie, S.P. King, C.P. Yau, P. Atienzar, J. Dane, P.E. Keivanidis, I. Zadrazil, D.D.C. Bradley, J. Nelson, Gravure printing inverted organic solar cells: the influence of ink properties on film quality and device performance, Sol. Energy Mater. Sol. C. 105 (2012) 77–85.
[8] C. Koidis, S. Logothetidis, S. Kassavetis, C. Kapnopoulos, P.G. Karagiannidis, D. Georgiou, A. Laskarakis, Effect of process parameters on the morphology and nanostructure of roll-to-roll printed P3HT:PCBM thin films for organic photovoltaics, Sol. Energy Mater. Sol. C. 112 (2013) 36–46.
[9] P.G. Karagiannidis, N. Kalfagiannis, D. Georgiou, A. Laskarakis, N.A. Hastas, C. Pitsalidis, S. Logothetidis, Effects of buffer layer properties and annealing process on bulk heterojunction morphology and organic solar cell performance, J. Mater. Chem. 22 (2012) 14624–14632.
[10] M. Sanyal, B. Schmidt-Hansberg, M.F.G. Klein, C. Munuera, A. Vorobiev, A. Colsmann, P. Scharfer, U. Lemmer, W. Schabel, H. Dosch, E. Barrena, Effect of photovoltaic polymer/fullerene blend composition ratio on microstructure evolution during film solidification investigated in real time by x-ray diffraction, Macromolecules 44 (2011) 3795–3800.
[11] M. Campoy-Quiles, T. Ferenczi, T. Agostinelli, P.G. Etchegoin, Y. Kim, T.D. Anthopoulos, P.N. Stavrinou, D.D.C. Bradley, J. Nelson, Morphology evolution via self-organization and lateral and vertical diffusion in polymer:fullerene solar cell blends, Nat. Mater. 7 (2008) 158–164.
[12] A. Orimo, K. Masuda, S. Honda, H. Benten, S. Ito, H. Ohkita, H. Tsuji, Surface segregation at the aluminum interface of poly(3-hexylthiophene)/fullerene solar cells, Appl. Phys. Lett. 96 (2010). 043305-1–043305-3.
[13] B.D. Cullity, Elements of X-Ray Diffraction, Addison-Wesley, Reading MA, 1956.
[14] T. Agostinelli, S. Lilliu, J.G. Labram, M. Campoy-Quiles, M. Hampton, E. Pires, J. Rawle, O. Bikondoa, D.D.C. Bradley, T.D. Anthopoulos, J. Nelson, J.E. Macdonald, Real-time investigation of crystallization and phase-segregation dynamics in P3HT:PCBM solar cells during thermal annealing, Adv. Funct. Mater. 21 (2011) 1701–1708.
[15] W.-H. Baek, H. Yang, T.-S. Yoon, C.J. Kang, H.H. Lee, Y.-S. Kim, Effect of P3HT:PCBM concentration in solvent on performances of organic solar cells, Sol. Energy Mater. Sol. C. 93 (2009) 1263–1267.
[16] S.S. van Bavel, E. Sourty, G. de With, J. Loos, Three-dimensional nanoscale organization of bulk heterojunction polymer solar cells, Nano Lett. 9 (2009) 507–513.
[17] G. Wang, S.-I. Na, T.-W. Kim, Y. Kim, S. Park, T. Lee, Effect of PEDOT:PSS–molecule interface on the charge transport characteristics of the large-area molecular electronic junctions, Org. Electron. 13 (2012) 771–777.
[18] M.A. Ibrahem, H.-Y. Wei, M.-H. Tsai, K.-C. Ho, J.-J. Shyue, C.W. Chu, Solution-processed zinc oxide nanoparticles as interlayer materials for inverted organic solar cells, Sol. Energy Mater. Sol. C. 108 (2013) 156–163.
[19] M.V. Madsen, K.O. Sylvester-Hvid, B. Dastmalchi, K. Hingerl, K. Norrman, T. Tromholt, M. Manceau, D. Angmo, F.C. Krebs, Ellipsometry as a nondestructive depth profiling tool for roll-to-roll manufactured flexible solar cells, J. Phys. Chem. C 115 (2011) 10817–10822.